ASTRONOMY

Mapping solar magnetic fields from the photosphere to the base of the corona

Ryohko Ishikawa[1]*, Javier Trujillo Bueno[2,3,4], Tanausú del Pino Alemán[2,3], Takenori J. Okamoto[1], David E. McKenzie[5], Frédéric Auchère[6], Ryouhei Kano[1], Donguk Song[1], Masaki Yoshida[1,7], Laurel A. Rachmeler[8], Ken Kobayashi[5], Hirohisa Hara[1], Masahito Kubo[1], Noriyuki Narukage[1], Taro Sakao[9], Toshifumi Shimizu[9], Yoshinori Suematsu[1], Christian Bethge[10], Bart De Pontieu[11,12,13], Alberto Sainz Dalda[11,14,15], Genevieve D. Vigil[5,16], Amy Winebarger[5], Ernest Alsina Ballester[17], Luca Belluzzi[17,18], Jiří Štěpán[19], Andrés Asensio Ramos[2,3], Mats Carlsson[12,13], Jorrit Leenaarts[20]

Routine ultraviolet imaging of the Sun's upper atmosphere shows the spectacular manifestation of solar activity; yet, we remain blind to its main driver, the magnetic field. Here, we report unprecedented spectropolarimetric observations of an active region plage and its surrounding enhanced network, showing circular polarization in ultraviolet (Mg II *h* & *k* and Mn I) and visible (Fe I) lines. We infer the longitudinal magnetic field from the photosphere to the very upper chromosphere. At the top of the plage chromosphere, the field strengths reach more than 300 G, strongly correlated with the Mg II *k* line core intensity and the electron pressure. This unique mapping shows how the magnetic field couples the different atmospheric layers and reveals the magnetic origin of the heating in the plage chromosphere.

INTRODUCTION

The chromosphere is a very important region of the solar atmosphere, with an extension of several thousand kilometers, located between the relatively cool surface layers of the photosphere and the overlying hot corona (*1*–*3*). Although the temperature of the chromospheric plasma does not exceed 10^4 K, the fact that its density is much larger than that of the extended and rarified corona implies that much more mechanical energy is required to sustain the chromosphere than the million-degree corona. Moreover, from the visible photospheric surface to the chromosphere-corona transition region (TR), the plasma density decreases exponentially by several orders of magnitude, more rapidly than the magnetic field strength. As a result, the $\beta = 1$ corrugated surface, where the ratio of gas to magnetic pressure is unity, lies inside the chromosphere. Above the $\beta = 1$ surface, the magnetic field essentially dominates the structuring and dynamics of the plasma. This, together with the fact that the nonthermal energy needed to heat the corona must propagate through the chromosphere, explains why it is indeed a crucial interface region to solve many of the key problems in solar and stellar physics.

It is impossible to fully understand the solar chromosphere without mapping its magnetic structure, especially in the relatively hot layers of the upper chromosphere and TR where $\beta < 1$ (*1*–*9*). To this end, we need to measure and model the polarization of ultraviolet spectral lines originating in such atmospheric regions (*10*). The theoretical investigations reported in the just quoted review paper led us to a series of suborbital space experiments called CLASP, which required the development of novel instrumentation (Supplementary Material 1A). The present investigation is based on a unique dataset acquired by the Chromospheric LAyer Spectropolarimeter (CLASP2), a suborbital space experiment that on 11 April 2019 allowed us to measure the first ever spectrally resolved Stokes profiles across the Mg II *h* & *k* lines in active and quiet regions of the solar disk.

METHODS

We focus on the CLASP2 measurements in an active region plage and its surrounding enhanced network (see Fig. 1, A and B, and note the position of the spectrograph's slit). These are poorly understood regions of the solar disk with large concentrations of magnetic flux, located at the footpoints of many coronal loops through which the mechanical energy that energizes the corona propagates (*3*, *11*). Although CLASP2 successfully measured the four Stokes parameters of several lines around 280 nm (see fig. S2), in this paper, we use only the intensity (Stokes *I*) and circular polarization (Stokes *V*) profiles of the Mg II *h* & *k* lines and of two nearby Mn I lines. The observed *V*/*I* spectra of these four lines can be seen in Fig. 1D, which also shows the detection of weaker circular polarization signals in other spectral lines. We point out that, in this paper, we always deal with the fractional circular polarization $V(\lambda)/I(\lambda)$ (hereafter, *V*/*I*), with λ being the wavelength.

[1]National Astronomical Observatory of Japan, Mitaka, Tokyo 181-8588, Japan. [2]Instituto de Astrofísica de Canarias, 38205 La Laguna, Tenerife, Spain. [3]Departamento de Astrofísica, Universidad de La Laguna, E-38206 La Laguna, Tenerife, Spain. [4]Consejo Superior de Investigaciones Científicas, Spain. [5]NASA Marshall Space Flight Center, Huntsville, AL 35812, USA. [6]Institut d'Astrophysique Spatiale, 91405 Orsay Cedex, France. [7]Department of Astronomical Science, School of Physical Sciences, SOKENDAI (The Graduate University for Advanced Studies), Mitaka, Tokyo 181-8588, Japan. [8]National Oceanic and Atmospheric Administration, National Centers for Environmental Information, Boulder, CO 80305, USA. [9]Institute of Space and Astronautical Science, Japan Aerospace Exploration Agency, Sagamihara, Kanagawa 252-5210, Japan. [10]Cooperative Institute for Research in Environmental Sciences, University of Colorado at Boulder, Boulder, CO 80305, USA. [11]Lockheed Martin Solar & Astrophysics Laboratory, Palo Alto, CA 94304, USA. [12]Rosseland Centre for Solar Physics, University of Oslo, NO-0315 Oslo, Norway. [13]Institute of Theoretical Astrophysics, University of Oslo, NO-0315 Oslo, Norway. [14]Bay Area Environmental Research Institute, Moffett Field, CA 94035, USA. [15]Stanford University, HEPL, Stanford, CA 94305-4085, USA. [16]Universities Space Research Association, Huntsville, AL 35805, USA. [17]Istituto Ricerche Solari Locarno, CH-6605 Locarno Monti, Switzerland. [18]Leibniz-Institut für Sonnenphysik (KIS), Schöneckstr. 6, D-79104, Freiburg, Germany. [19]Astronomical Institute, Academy of Sciences of the Czech Republic, 25165 Ondrejov, Czech Republic. [20]Institute for Solar Physics, Department of Astronomy, Stockholm University, AlbaNova University Centre, SE-106 91, Stockholm, Sweden.
*Corresponding author. Email: ryoko.ishikawa@nao.ac.jp

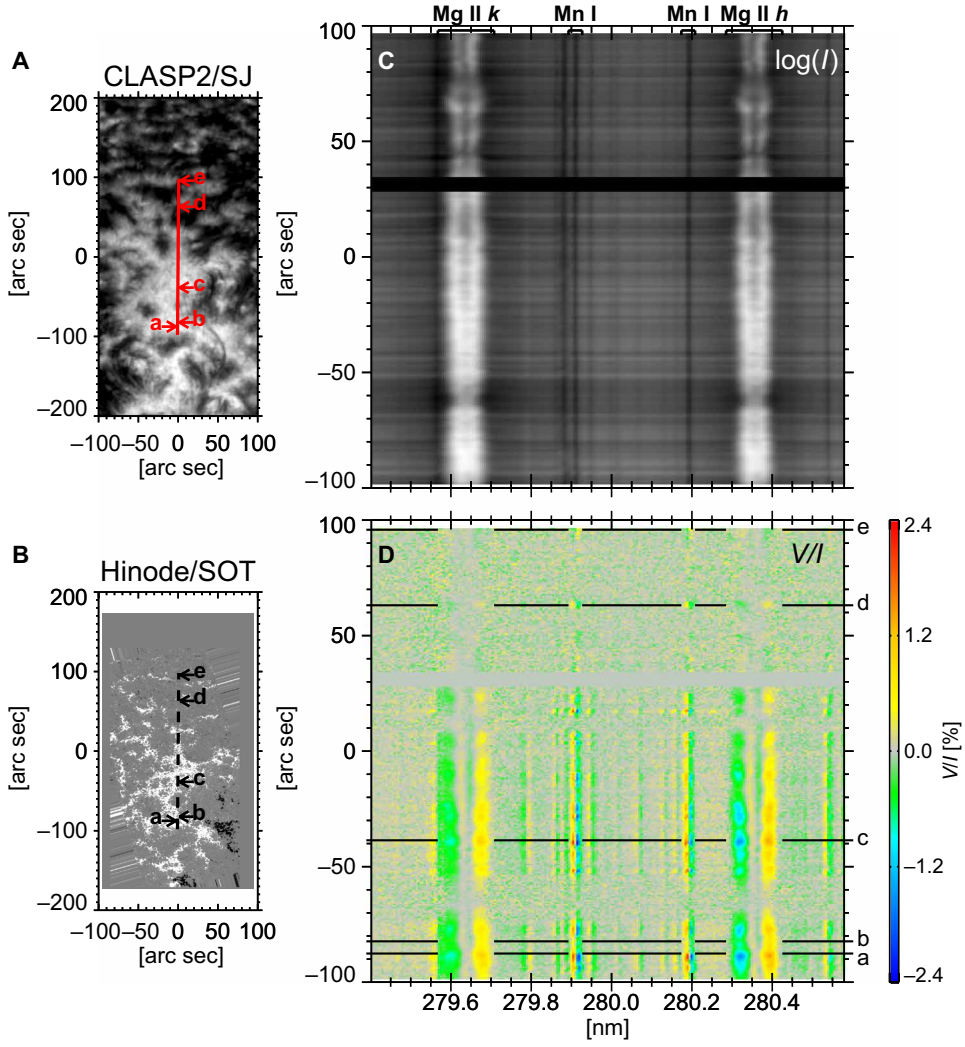

Fig. 1. CLASP2 and Hinode data. (**A**) Broadband Lyman-α image obtained by the CLASP2 slit-jaw system. The red line indicates the radially oriented slit of the CLASP2 spectrograph, which covers 196 arc sec. (**B**) Longitudinal component of the photospheric magnetic field inferred from the Stokes profiles observed by Hinode/SOT-SP in Fe I visible lines. (**C**) Variation along the slit of the intensity profile $I(\lambda)$ observed in the spectral region of the Mg II *h* & *k* lines. The labels at the top of (C) indicate the location of Mg II *k* at 279.64 nm, Mg II *h* at 280.35 nm, and the Mn I lines at 279.91 and 280.19 nm. (**D**) Fractional circular polarization $V(\lambda)/I(\lambda)$ observed by CLASP2 around 280 nm. The *I* and *V*/*I* spectra are the result of temporally averaging the individual Stokes parameters during 150.4 s. The vertical axes indicate the distance in arc seconds along the spatial direction of the CLASP2 slit, measured from its center. The small gap seen in (C) and (D) results from the lack of data in a few deteriorated pixels.

CLASP2 detected clear circular polarization signals not only within the bright region of the plage but also at the enhanced network elements located at d and e (Fig. 1A). The Stokes *V*/*I* profiles of the Mg II *h* & *k* resonance lines have two external lobes and two inner lobes, which encode information on the longitudinal component of the magnetic field in the middle chromosphere and at the top of the upper chromosphere, respectively (Supplementary Materials 2A to 2C). The *V*/*I* profiles of the two Mn I lines at 279.91 nm and at 280.19 nm have only two lobes, which provide information on the longitudinal field component in the lower chromosphere (Supplementary Material 2D). In addition, to obtain the longitudinal field component in the underlying photosphere, we have used the Stokes profiles of two visible Fe I lines measured by the Hinode spacecraft during the CLASP2 flight (Supplementary Material 1B).

All such circular polarization signals are produced by the Zeeman effect caused by the magnetic field that permeates the solar atmosphere. To determine the longitudinal field component from the Stokes *I* and *V* profiles measured by CLASP2 in the abovementioned chromospheric lines, we applied the weak field approximation (WFA; Supplementary Material 1D). Figure 2 shows an example of the observed profiles, with the colored curves indicating the corresponding WFA fits. The generally stronger photospheric magnetic field values reported here result from the application of a suitable inversion code to the Stokes profiles observed by the Hinode spacecraft (Supplementary Material 1E).

RESULTS AND DISCUSSION

Figure 3 gives the variation, along the spatial direction of the spectrograph's slit, of the longitudinal component of the magnetic field. The figure shows this quantity in the photosphere (green curves), in the lower chromosphere (blue symbols), in the middle chromosphere

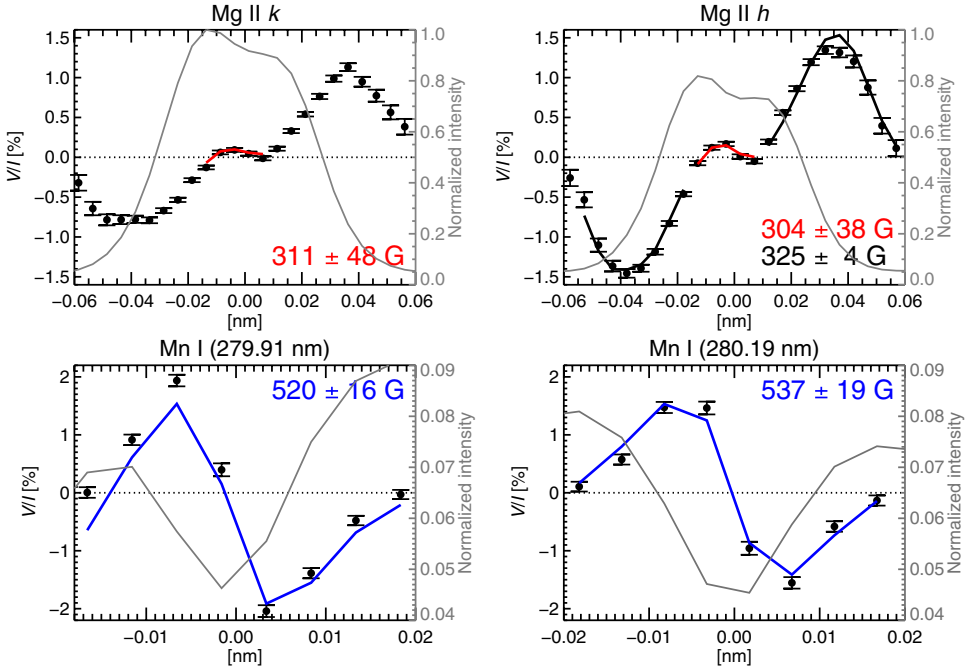

Fig. 2. Example of the Stokes *I* and *V*/*I* profiles observed by CLASP2. The profiles correspond to Mg II *k* at 279.64 nm, Mg II *h* at 280.35 nm, Mn I at 279.91 nm, and Mn I at 280.19 nm at location c in Fig. 1, where the longitudinal field retrieved from the Mg II *h* & *k* lines is among the strongest ones. The gray curves show the corresponding Stokes *I* profiles, normalized to the maximum intensity of the Mg II *k* line. The *V*/*I* error bars indicate the ±1σ uncertainties resulting from the photon noise. The WFA fits and the inferred longitudinal magnetic field values are shown in blue for the Mn I lines, in black for the external *V*/*I* lobes of Mg II *h*, and in red for the inner *V*/*I* lobes of Mg II *h* & *k*.

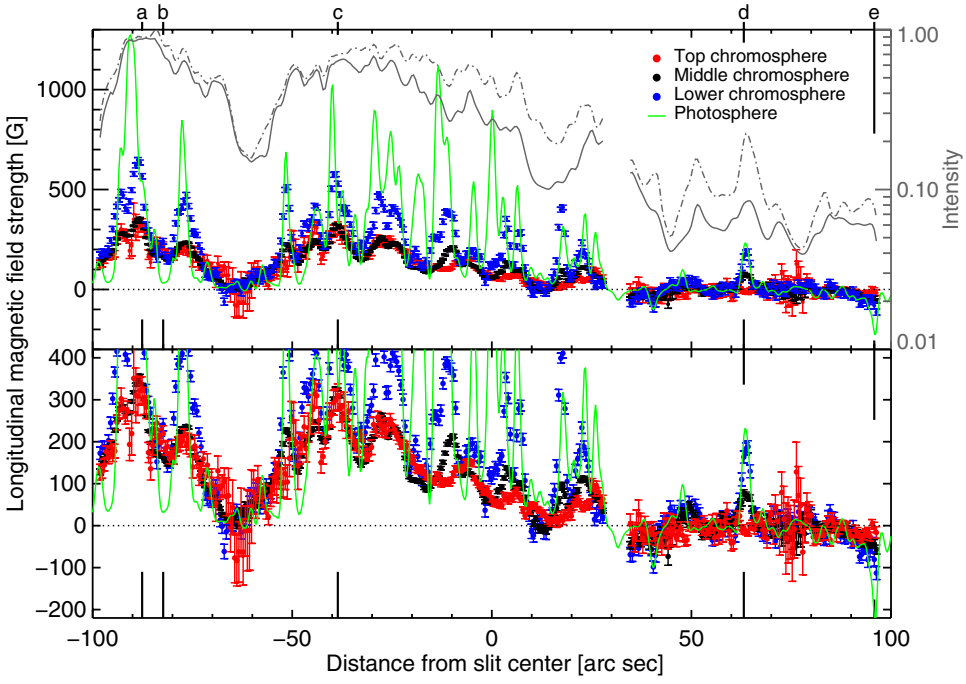

Fig. 3. Spatial variation of the longitudinal component of the magnetic field (B_L). Blue symbols: B_L in the lower chromosphere determined from the Mn I lines. Black symbols: B_L in the middle chromosphere determined from the external lobes of the *V*/*I* profiles in the Mg II *h* line. Red symbols: B_L at the top of the upper chromosphere determined from the inner lobes of the *V*/*I* profiles in the Mg II *h* & *k* lines. Green curve: B_L in the photosphere obtained from the Hinode/SOT-SP observations, after spatially smearing the data to mimic the CLASP2 resolution (Supplementary Material 1E). The error bars of the CLASP2 data represent 1σ errors. Note that the thin black curves give the normalized intensity observed by CLASP2 at the k_3 line center and at the k_{2v} emission peak of the Mg II *k* line (solid and dashed-dotted; see the inset of fig. S4). The lower panel is a zoomed-in image of the upper one.

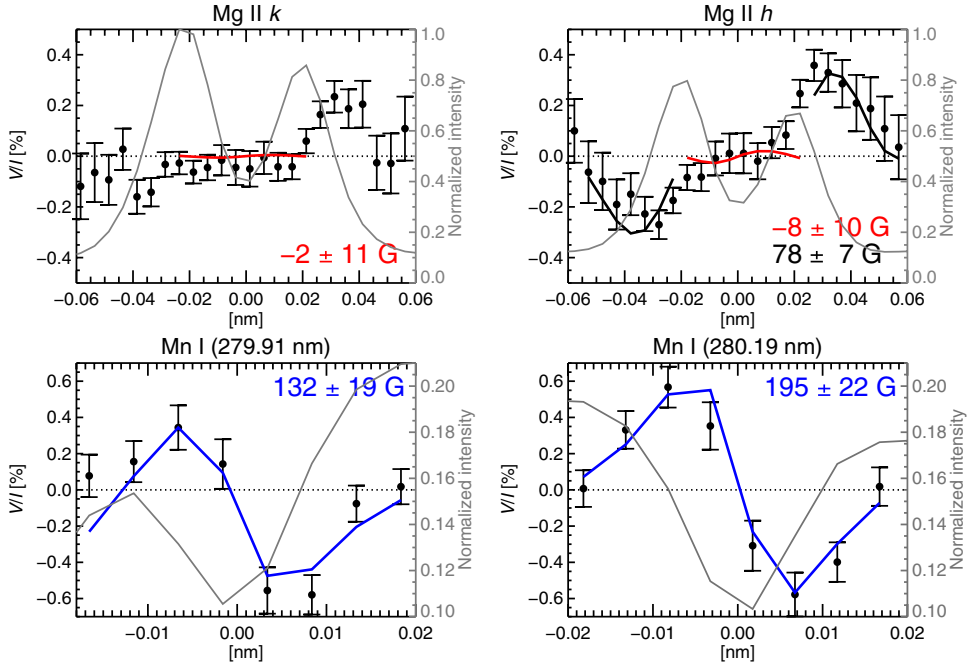

Fig. 4. CLASP2 data corresponding to one of the network features. *V/I* profiles at location d indicated in Fig. 1. See the caption of Fig. 2 for further explanation. We find $B_L = -5 \pm 7$ G at the top of the upper chromosphere (after averaging the longitudinal field values retrieved from the inner *V/I* lobes of the Mg II *h* & *k* lines), $B_L = 78 \pm 7$ G in the middle chromosphere (from the external *V/I* lobes of Mg II *h*), and $B_L = 164 \pm 15$ G in the lower chromosphere (from the *V/I* profiles of the Mn I lines).

Table 1. Correlation coefficients (CI for intensity and CP for electron pressure). The table gives the correlation coefficient between the longitudinal component of the magnetic field, B_L, inferred at different heights in the atmosphere, and (i) the observed Mg II *k*-line intensity (k_3 or k_{2v}) and (ii) the inferred electron pressure near the upper chromosphere (see Supplementary Material 2E). The linear Pearson correlation coefficients have been calculated considering only the bright plage region pixels located between −98 and +28 arc sec (see Fig. 1C).

Wavelength window for B_L	Atmospheric layer	CI (k_3)	CI (k_{2v})	CP
Inner lobes of Mg II *h* & *k*	Top of upper chromosphere	0.87	0.81	0.74
External lobes of Mg II *h*	Middle chromosphere	0.80	0.75	0.67
Mn I lines around 280 nm	Lower chromosphere	0.65	0.63	0.55
Fe I lines around 630.2 nm	Photosphere	0.48	0.44	

(black symbols), and at the top of the upper chromosphere (red symbols). Note that the error bars (1σ) of the inferred values, due to the noise in *V/I*, are very small, thanks to the high-precision of the CLASP2 measurements. The observed bright plage region extends from −98 arc sec to about 28 arc sec, with a small dark region located around −62 arc sec (see Fig. 1A).

In the bright plage region, we see clearly in Fig. 3 that the magnetic field always shows a single magnetic polarity, except perhaps at the −65 and +12 arc sec positions, where the retrieved opposite polarity fields may not be statistically significant because they are comparable to or smaller than the 1σ uncertainty. As expected, the strongest magnetic fields are found in the photosphere of the observed plage, where the magnetic field appears to be organized into small regions with strong magnetic concentrations (with longitudinal field components as large as 1250 G) separated by small regions with longitudinal field values of the order of 10 G (see the green curve and its spatial fluctuation, which has typical scales of less than 10 arc sec). In the lower chromosphere (blue symbols), the magnetic field also shows a substantial fluctuation on similar spatial scales, but the amplitude of the spatial variation is considerably smaller, and this variation is not exactly in phase with the one in the underlying photosphere (e.g., note that the spatial locations of the blue-symbol peaks do not coincide exactly with those of the green curve). In the low chromosphere, the maximum longitudinal magnetic field values are about 700 G (blue symbols). In the middle chromosphere of the plage and at the top of its upper chromosphere, the black and red symbols of Fig. 3 indicate that the longitudinal component of the magnetic field varies from almost 0 G (slit positions around +12 and −65 arc sec) to more than 300 G (locations a, c and −44 arc sec), showing a smoother spatial variation than in the lower chromosphere (blue symbols) and photosphere (green curve). The longitudinal magnetic field values found near the TR (red symbols, inferred from the inner lobes of the Stokes *V/I* profiles of Mg II *h* & *k*) are not much weaker than those found in the middle chromosphere (black symbols, determined from the outer *V/I* lobes of the *h* line), although it must be noted that the latter values are a lower limit (Supplementary Material 2C). Last, note that at almost all of the spatial positions where the fluctuating green curve reaches

its local minima, the photospheric longitudinal field values are smaller than at the same locations in the overlying layers (e.g., see position b and the corresponding fig. S5). However, at the spatial positions where the longitudinal component of the magnetic field in the lower chromosphere (blue symbols) reaches its smallest values, we find similar ones in the middle chromosphere and at the top of the upper chromosphere (black and red symbols, respectively). These and the previously mentioned fact, namely, that the spatial fluctuations of the longitudinal field values decrease with height, confirm that the plage magnetic field is highly structured in the photosphere, with strong and weak field variations, and that it expands rapidly, merging and spreading horizontally in the overlying chromosphere where the field is weaker and has smoother spatial variations.

We have found a remarkably high correlation between the longitudinal component of the magnetic field in the middle and top layers of the plage chromosphere and the intensity at the center and the emission peaks of the Mg II *k* line (see Fig. 3). As shown in Table 1, the coefficient that quantifies this correlation increases with height in the plage atmosphere, and it is important to note that the intensity in the *k* line-core emission peaks correlates with the temperature at its formation height (*12*). Moreover, from inversions of the observed Mg II *h* & *k* intensity profiles (Supplementary Material 2E), we have found (see Table 1) that in the middle and the upper chromosphere, the longitudinal component of the magnetic field is also substantially correlated with the electron pressure (i.e., with the product of the temperature and the electron density). These pieces of empirical information strongly support the idea that the heating of the upper chromosphere of active region plages is of magnetic origin.

Consider now the supergranulation cell outlined by its bright chromospheric network, which is located above 60 arc sec in Fig. 1A. The slit of the spectrograph crosses network features at 63 arc sec (location d) and at 97 arc sec (location e). As shown by the green curve of Fig. 3, the longitudinal component of the magnetic field in the photosphere of these two network elements is about 220 G. At these network locations, we find longitudinal field strengths of about 160 and 80 G in the lower and middle chromosphere, respectively (see Fig. 4 for location d). Figure 3 shows that the magnetic fields in the atmospheres of these two network elements have opposite polarities. As seen in the top panels of Fig. 4, the inner lobes of the Stokes *V*/*I* profiles of the *h* & *k* lines are so weak that their circular polarization amplitudes are compatible with zero within the error bars, and this is not due to cancelations of the circular polarization signals during the 150.4-s integration time (Supplementary Material 1D). The absence of appreciable inner lobes in such *V*/*I* profiles leads us to conclude that the magnetic field in the very upper chromosphere of the observed network features is weaker than about 10 G. Therefore, in the atmospheres of these network elements, the longitudinal field values vary approximately from 220 G in the photosphere to 160 G in the lower chromosphere, to at least 80 G in the middle chromosphere, and to less than 10 G at the top of the upper chromosphere.

We foresee three possible scenarios compatible with the abovementioned results from the CLASP2 spectropolarimetric observations of the network features: (i) the magnetic loops of the network do not reach the very top of the chromosphere and return to the photosphere after reaching chromospheric heights, (ii) the magnetic fields in the very upper chromosphere of the network regions are too weak to be detected through the Zeeman effect in the Mg II resonance lines, and (iii) the magnetic field in the top layers of the network chromosphere becomes nearly perpendicular to the lines of sight of the CLASP2 observation, so that there is hardly any longitudinal field component to measure. Our CLASP2 circular polarization measurements provide quantitative evidence that the commonly held picture of a wine glass–shaped magnetic canopy of network fields that fill the entire quiet solar chromosphere above a certain height is too simplistic to describe the expansion of the magnetic field in the observed enhanced network regions (*13*, *14*). An advanced inversion code is currently under development, and we hope that its future application to the four Stokes profiles observed by CLASP2 (see fig. S2) will allow us to disentangle among the three options mentioned above.

Although a suborbital space experiment can only provide a few minutes of observing time, the unprecedented observations achieved by CLASP2 have demonstrated the enormous diagnostic potential of spectropolarimetry in the spectral region of the Mg II *h* & *k* lines. Of particular interest are the circular polarization signals observed in the Mg II and Mn I resonance lines. This is the first time that the longitudinal component of the magnetic field is simultaneously determined at several heights from the photosphere to the very top layers of the chromosphere of active region plages and enhanced network features, at each position along the spatial direction of the spectrograph's slit. This opens up the possibility of mapping the magnetic field throughout the solar atmosphere over large fields of view, an empirical information that is crucial for obtaining more accurate coronal field estimates and for deciphering how the magnetic field couples the different atmospheric layers and channels the mechanical energy that heats the chromosphere and the corona of our nearest star.

SUPPLEMENTARY MATERIALS

Supplementary material for this article is available at http://advances.sciencemag.org/cgi/content/full/7/8/eabe8406/DC1

REFERENCES AND NOTES

1. J. W. Harvey, Chromospheric magnetic fields. *Astron. Soc. Pac. Conf. Ser.* **405**, 157 (2009).
2. R. J. Rutten, The quiet-Sun photosphere and chromosphere. *Phil. Trans. R. Soc. A* **370**, 3129–3150 (2012).
3. M. Carlsson, B. De Pontieu, V. H. Hansteen, New view of the solar chromosphere. *Annu. Rev. Astron. Astrophys.* **57**, 189–226 (2019).
4. E. N. Parker, *Conversations on Electric and Magnetic Fields in the Cosmos* (Princeton Univ. Press, 2007).
5. B. V. Gudiksen, Å. Nordlund, An ab initio approach to the solar coronal heating problem. *Astrophys. J.* **618**, 1020–1030 (2005).
6. B. De Pontieu, S. W. McIntosh, M. Carlsson, V. H. Hansteen, T. D. Tarbell, C. J. Schrijver, A. M. Title, R. A. Shine, S. Tsuneta, Y. Katsukawa, K. Ichimoto, Y. Suematsu, T. Shimizu, S. Nagata, Chromospheric Alfvénic waves strong enough to power the solar wind. *Science* **318**, 1574–1577 (2007).
7. H. Isobe, M. R. E. Proctor, N. O. Weiss, Convection-driven emergence of small-scale magnetic fields and their role in coronal heating and solar wind acceleration. *Astrophys. J.* **679**, L57–L60 (2008).
8. J. W. Cirtain, L. Golub, A. R. Winebarger, B. de Pontieu, K. Kobayashi, R. L. Moore, R. W. Walsh, K. E. Korreck, M. Weber, P. McCauley, A. Title, S. Kuzin, C. E. DeForest, Energy release in the solar corona from spatially resolved magnetic braids. *Nature* **493**, 501–503 (2013).
9. J. Martínez-Sykora, B. De Pontieu, V. H. Hansteen, L. Rouppe van der Voort, M. Carlsson, T. M. D. Pereira, On the generation of solar spicules and Alfvénic waves. *Science* **356**, 1269–1272 (2017).
10. J. Trujillo Bueno, E. Landi Degl'Innocenti, L. Belluzzi, The physics and diagnostic potential of ultraviolet spectropolarimetry. *Space Sci. Rev.* **210**, 183–226 (2017).
11. F. Kneer, Chromosphere of active regions on the Sun. *Mem. Soc. Astron. Ital.* **81**, 604 (2010).
12. J. Leenaarts, T. M. D. Pereira, M. Carlsson, H. Uitenbroek, B. De Pontieu, The formation of IRIS diagnostics. II. The formation of the Mg II h&k lines in the solar atmosphere. *Astrophys. J.* **772**, 90 (2013).

13. C. J. Schrijver, A. M. Title, The magnetic connection between the solar photosphere and the corona. *Astrophys. J.* **597**, L165–L168 (2003).
14. S. Wedemeyer-Böhm, A. Lagg, Å. Nordlund, Coupling from the photosphere to the chromosphere and the corona, in *The Origin and Dynamics of Solar Magnetism*, M. J. Thompson, A. Balogh, J. L. Culhane, Å. Nordlund, S. K. Solanki, J. P. Zahn, Eds. (Springer, 2009), vol. 32 of Space Sciences Series of ISSI, p. 317.
15. R. Ishikawa, R. Kano, T. Bando, Y. Suematsu, S.-n. Ishikawa, M. Kubo, N. Narukage, H. Hara, S. Tsuneta, H. Watanabe, K. Ichimoto, K. Aoki, K. Miyagawa, Birefringence of magnesium fluoride in the vacuum ultraviolet and application to a half-waveplate. *Appl. Optics* **52**, 8205–8211 (2013).
16. R. Ishikawa, N. Narukage, M. Kubo, S. Ishikawa, R. Kano, S. Tsuneta, Strategy for realizing high-precision VUV spectro-polarimeter. *Solar Phys.* **289**, 4727–4747 (2014).
17. N. Narukage, F. Auchère, R. Ishikawa, R. Kano, S. Tsuneta, A. R. Winebarger, K. Kobayashi, Vacuum ultraviolet spectropolarimeter design for precise polarization measurements. *Appl. Optics* **54**, 2080–2084 (2015).
18. S. Ishikawa, T. Shimizu, R. Kano, T. Bando, R. Ishikawa, G. Giono, S. Tsuneta, S. Nakayama, T. Tajima, Development of a precise polarization modulator for UV spectropolarimetry. *Solar Phys.* **290**, 3081–3088 (2015).
19. G. Giono, R. Ishikawa, N. Narukage, R. Kano, Y. Katsukawa, M. Kubo, S. Ishikawa, T. Bando, H. Hara, Y. Suematsu, A. Winebarger, K. Kobayashi, F. Auchère, J. Trujillo Bueno, Polarization calibration of the *Chromospheric Lyman-Alpha SpectroPolarimeter* for a 0.1% polarization sensitivity in the VUV range. Part I: Pre-flight calibration. *Solar Phys.* **291**, 3831–3867 (2016).
20. G. Giono, R. Ishikawa, N. Narukage, R. Kano, Y. Katsukawa, M. Kubo, S. Ishikawa, T. Bando, H. Hara, Y. Suematsu, A. Winebarger, K. Kobayashi, F. Auchère, J. Trujillo Bueno, S. Tsuneta, T. Shimizu, T. Sakao, J. Cirtain, P. Champey, A. Asensio Ramos, J. Štěpán, L. Belluzzi, R. Manso Sainz, B. De Pontieu, K. Ichimoto, M. Carlsson, R. Casini, M. Goto, Polarization calibration of the *Chromospheric Lyman-Alpha SpectroPolarimeter* for a 0.1% polarization sensitivity in the VUV range. Part II: In-flight calibration. *Solar Phys.* **292**, 57 (2017).
21. R. Kano, J. Trujillo Bueno, A. Winebarger, F. Auchère, N. Narukage, R. Ishikawa, K. Kobayashi, T. Bando, Y. Katsukawa, M. Kubo, S. Ishikawa, G. Giono, H. Hara, Y. Suematsu, T. Shimizu, T. Sakao, S. Tsuneta, K. Ichimoto, M. Goto, L. Belluzzi, J. Štěpán, A. Asensio Ramos, R. Manso Sainz, P. Champey, J. Cirtain, B. De Pontieu, R. Casini, M. Carlsson, Discovery of scattering polarization in the hydrogen Lyα line of the solar disk radiation. *Astrophys. J. Lett.* **839**, L10 (2017).
22. R. Ishikawa, J. Trujillo Bueno, H. Uitenbroek, M. Kubo, S. Tsuneta, M. Goto, R. Kano, N. Narukage, T. Bando, Y. Katsukawa, S. Ishikawa, G. Giono, Y. Suematsu, H. Hara, T. Shimizu, T. Sakao, A. Winebarger, K. Kobayashi, J. Cirtain, P. Champey, F. Auchère, J. Štěpán, L. Belluzzi, A. Asensio Ramos, R. Manso Sainz, B. De Pontieu, K. Ichimoto, M. Carlsson, R. Casini, Indication of the Hanle effect by comparing the scattering polarization observed by CLASP in the Lyα and Si III 120.65 nm lines. *Astrophys. J.* **841**, 31 (2017).
23. J. Štěpán, J. Trujillo Bueno, L. Belluzzi, A. Asensio Ramos, R. Manso Sainz, T. del Pino Alemán, R. Casini, R. Kano, A. Winebarger, F. Auchère, R. Ishikawa, N. Narukage, K. Kobayashi, T. Bando, Y. Katsukawa, M. Kubo, S. Ishikawa, G. Giono, H. Hara, Y. Suematsu, T. Shimizu, T. Sakao, S. Tsuneta, K. Ichimoto, J. Cirtain, P. Champey, B. De Pontieu, M. Carlsson, A statistical inference method for interpreting the CLASP observations. *Astrophys. J.* **865**, 48 (2018).
24. J. Trujillo Bueno, J. Štěpán, L. Belluzzi, A. Asensio Ramos, R. Manso Sainz, T. del Pino Alemán, R. Casini, R. Ishikawa, R. Kano, A. Winebarger, F. Auchère, N. Narukage, K. Kobayashi, T. Bando, Y. Katsukawa, M. Kubo, S. Ishikawa, G. Giono, H. Hara, Y. Suematsu, T. Shimizu, T. Sakao, S. Tsuneta, K. Ichimoto, J. Cirtain, P. Champey, B. De Pontieu, M. Carlsson, CLASP constraints on the magnetization and geometrical complexity of the chromosphere-corona transition region. *Astrophys. J.* **866**, L15 (2018).
25. T. Tsuzuki, R. Ishikawa, R. Kano, N. Narukage, D. Song, M. Yoshida, F. Uraguchi, T. J. Okamoto, D. McKenzie, K. Kobayashi, L. Rachmeler, F. Auchère, J. Trujillo Bueno, Optical design of the Chromospheric LAyer Spectro-Polarimeter (CLASP2). *Proc. SPIE* **11444**, 114446W (2020).
26. M. Yoshida, D. Song, R. Ishikawa, R. Kano, Y. Katsukawa, Y. Suematsu, N. Narukage, M. Kubo, K. Shinoda, T. J. Okamoto, D. E. McKenzie, L. A. Rachmeler, F. Auchère, J. Trujillo Bueno, Wavefront error measurements and alignment of CLASP2 telescope with a dual-band pass cold mirror coated primary mirror. *Proc. SPIE* **10699**, 1069930 (2018).
27. D. Song, R. Ishikawa, R. Kano, M. Yoshida, T. Tsuzuki, F. Uraguchi, K. Shinoda, H. Hara, T. J. Okamoto, F. Auchère, D. E. McKenzie, L. A. Rachmeler, J. Trujillo Bueno, Optical alignment of the high-precision UV spectro-polarimeter (CLASP2). *Proc. SPIE* **10699**, 106992W (2018).
28. J. O. Stenflo, D. Dravins, N. Wihlborg, A. Bruns, V. K. Prokof'ev, I. A. Zhitnik, H. Biverot, L. Stenmark, Search for spectral line polarization in the solar vacuum ultraviolet. *Solar Phys.* **66**, 13–19 (1980).
29. E. Tandberg-Hanssen, C. C. Cheng, R. G. Athay, J. M. Beckers, J. C. Brandt, R. D. Chapman, E. C. Bruner, W. Henze, C. L. Hyder, J. B. Gurman, Preliminary observations and results obtained with the ultraviolet spectrometer and polarimeter. *Astrophys. J.* **244**, L127–L132 (1981).
30. W. Henze Jr., E. Tandberg-Hanssen, M. J. Hagyard, B. E. Woodgate, R. A. Shine, J. M. Beckers, M. Bruner, J. B. Gurman, C. L. Hyder, E. A. West, Observations of the longitudinal magnetic field in the transition region and photosphere of a sunspot. *Solar Phys.* **81**, 231–244 (1982).
31. M. J. Hagyard, D. Teuber, E. A. West, E. Tandberg-Hanssen, W. Henze Jr., J. M. Beckers, M. Bruner, C. L. Hyder, B. E. Woodgate, Vertical gradients of sunspot magnetic fields. *Solar Phys.* **84**, 13–31 (1983).
32. W. Henze, J. O. Stenflo, Polarimetry in the Mg II h and k lines. *Solar Phys.* **111**, 243–254 (1987).
33. R. Manso Sainz, T. del Pino Alemán, R. Casini, S. McIntosh, Spectropolarimetry of the solar Mg II h and k lines. *Astrophys. J. Lett.* **883**, L30 (2019).
34. M. Kubo, Y. Katsukawa, Y. Suematsu, R. Kano, T. Bando, N. Narukage, R. Ishikawa, H. Hara, G. Giono, S. Tsuneta, S. Ishikawa, T. Shimizu, T. Sakao, A. Winebarger, K. Kobayashi, J. Cirtain, P. Champey, F. Auchère, J. Trujillo Bueno, A. Asensio Ramos, J. Štěpán, L. Belluzzi, R. Manso Sainz, B. De Pontieu, K. Ichimoto, M. Carlsson, R. Casini, M. Goto, Discovery of ubiquitous fast-propagating intensity disturbances by the Chromospheric Lyman Alpha Spectropolarimeter (CLASP). *Astrophys. J.* **832**, 141 (2016).
35. L. Belluzzi, J. Trujillo Bueno, The polarization of the solar Mg II *h* and *k* lines. *Astrophys. J. Lett.* **750**, L11 (2012).
36. E. Alsina Ballester, L. Belluzzi, J. Trujillo Bueno, The magnetic sensitivity of the Mg II *k* line to the joint action of Hanle, Zeeman, and magneto-optical effects. *Astrophys. J. Lett.* **831**, L15 (2016).
37. T. del Pino Alemán, R. Casini, R. Manso Sainz, Magnetic diagnostics of the solar chromosphere with the Mg II h-k lines. *Astrophys. J. Lett.* **830**, L24 (2016).
38. T. del Pino Alemán, J. Trujillo Bueno, R. Casini, R. Manso Sainz, The magnetic sensitivity of the resonance and subordinate lines of Mg II in the solar chromosphere. *Astrophys. J.* **891**, 91 (2020).
39. T. Kosugi, K. Matsuzaki, T. Sakao, T. Shimizu, Y. Sone, S. Tachikawa, T. Hashimoto, K. Minesugi, A. Ohnishi, T. Yamada, S. Tsuneta, H. Hara, K. Ichimoto, Y. Suematsu, M. Shimojo, T. Watanabe, S. Shimada, J. M. Davis, L. D. Hill, J. K. Owens, A. M. Title, J. L. Culhane, L. K. Harra, G. A. Doschek, L. Golub, The *Hinode* (Solar-B) mission: An overview. *Solar Phys.* **243**, 3–17 (2007).
40. K. Ichimoto, B. Lites, D. Elmore, Y. Suematsu, S. Tsuneta, Y. Katsukawa, T. Shimizu, R. Shine, T. Tarbell, A. Title, J. Kiyohara, K. Shinoda, G. Card, A. Lecinski, K. Streander, M. Nakagiri, M. Miyashita, M. Noguchi, C. Hoffmann, T. Cruz, Polarization calibration of the solar optical telescope onboard *Hinode*. *Solar Phys.* **249**, 233–261 (2008).
41. B. W. Lites, D. L. Akin, G. Card, T. Cruz, D. W. Duncan, C. G. Edwards, D. F. Elmore, C. Hoffmann, Y. Katsukawa, N. Katz, M. Kubo, K. Ichimoto, T. Shimizu, R. A. Shine, K. V. Streander, A. Suematsu, T. D. Tarbell, A. M. Title, S. Tsuneta, The *Hinode Spectro-Polarimeter*. *Solar Phys.* **283**, 579–599 (2013).
42. S. Tsuneta, K. Ichimoto, Y. Katsukawa, S. Nagata, M. Otsubo, T. Shimizu, Y. Suematsu, M. Nakagiri, M. Noguchi, T. Tarbell, A. Title, R. Shine, W. Rosenberg, C. Hoffmann, B. Jurcevich, G. Kushner, M. Levay, B. Lites, D. Elmore, T. Matsushita, N. Kawaguchi, H. Saito, I. Mikami, L. D. Hill, J. K. Owens, The solar optical telescope for the *Hinode* mission: An overview. *Solar Phys.* **249**, 167–196 (2008).
43. Y. Suematsu, S. Tsuneta, K. Ichimoto, T. Shimizu, M. Otsubo, Y. Katsukawa, M. Nakagiri, M. Noguchi, T. Tamura, Y. Kato, H. Hara, M. Kubo, I. Mikami, H. Saito, T. Matsushita, N. Kawaguchi, T. Nakaoji, K. Nagae, S. Shimada, N. Takeyama, T. Yamamuro, The solar optical telescope of solar-B (Hinode): The optical telescope assembly. *Solar Phys.* **249**, 197–220 (2008).
44. T. Shimizu, S. Nagata, S. Tsuneta, T. Tarbell, C. Edwards, R. Shine, C. Hoffmann, E. Thomas, S. Sour, R. Rehse, O. Ito, Y. Kashiwagi, M. Tabata, K. Kodeki, M. Nagase, K. Matsuzaki, K. Kobayashi, K. Ichimoto, Y. Suematsu, Image stabilization system for *Hinode* (Solar-B) solar optical telescope. *Solar Phys.* **249**, 221–232 (2008).
45. J. R. Lemen, A. M. Title, D. J. Akin, P. F. Boerner, C. Chou, J. F. Drake, D. W. Duncan, C. G. Edwards, F. M. Friedlaender, G. F. Heyman, N. E. Hurlburt, N. L. Katz, G. D. Kushner, M. Levay, R. W. Lindgren, D. P. Mathur, E. L. McFeaters, S. Mitchell, R. A. Rehse, C. J. Schrijver, L. A. Springer, R. A. Stern, T. D. Tarbell, J.-P. Wuelser, C. J. Wolfson, C. Yanari, J. A. Bookbinder, P. N. Cheimets, D. Caldwell, E. E. Deluca, R. Gates, L. Golub, S. Park, W. A. Podgorski, R. I. Bush, P. H. Scherrer, M. A. Gummin, P. Smith, G. Auker, P. Jerram, P. Pool, R. Soufli, D. L. Windt, S. Beardsley, M. Clapp, J. Lang, N. Waltham, The *Atmospheric Imaging Assembly* (AIA) on the *Solar Dynamics Observatory* (SDO). *Solar Phys.* **275**, 17–40 (2012).
46. P. H. Scherrer, J. Schou, R. I. Bush, A. G. Kosovichev, R. S. Bogart, J. T. Hoeksema, Y. Liu, T. L. Duvall Jr., J. Zhao, A. M. Title, C. J. Schrijver, T. D. Tarbell, S. Tomczyk, The *Helioseismic and Magnetic Imager* (HMI) investigation for the *Solar Dynamics Observatory* (SDO). *Solar Phys.* **275**, 207–227 (2012).

47. W. D. Pesnell, B. J. Thompson, P. C. Chamberlin, The *Solar Dynamics Observatory* (SDO). *Solar Phys.* **275**, 3–15 (2012).
48. B. De Pontieu, A. M. Title, J. R. Lemen, G. D. Kushner, D. J. Akin, B. Allard, T. Berger, P. Boerner, M. Cheung, C. Chou, J. F. Drake, D. W. Duncan, S. Freeland, G. F. Heyman, C. Hoffman, N. E. Hurlburt, R. W. Lindgren, D. Mathur, R. Rehse, D. Sabolish, R. Seguin, C. J. Schrijver, T. D. Tarbell, J.-P. Wülser, C. J. Wolfson, C. Yanari, J. Mudge, N. Nguyen-Phuc, R. Timmons, R. van Bezooijen, I. Weingrod, R. Brookner, G. Butcher, B. Dougherty, J. Eder, V. Knagenhjelm, S. Larsen, D. Mansir, L. Phan, P. Boyle, P. N. Cheimets, E. E. DeLuca, L. Golub, R. Gates, E. Hertz, S. McKillop, S. Park, T. Perry, W. A. Podgorski, K. Reeves, S. Saar, P. Testa, H. Tian, M. Weber, C. Dunn, S. Eccles, S. A. Jaeggli, C. C. Kankelborg, K. Mashburn, N. Pust, L. Springer, R. Carvalho, L. Kleint, J. Marmie, E. Mazmanian, T. M. D. Pereira, S. Sawyer, J. Strong, S. P. Worden, M. Carlsson, V. H. Hansteen, J. Leenaarts, M. Wiesmann, J. Aloise, K.-C. Chu, R. I. Bush, P. H. Scherrer, P. Brekke, J. Martinez-Sykora, B. W. Lites, S. W. McIntosh, H. Uitenbroek, T. J. Okamoto, M. A. Gummin, G. Auker, P. Jerram, P. Pool, N. Waltham, The *Interface Region Imaging Spectrograph* (IRIS). *Solar Phys.* **289**, 2733–2779 (2014).
49. J. Jefferies, B. W. Lites, A. Skumanich, Transfer of line radiation in a magnetic field. *Astrophys. J.* **343**, 920–935 (1989).
50. E. Landi Degl'Innocenti, M. Landolfi, *Polarization in Spectral Lines* (Springer, 2004), vol. 307 of Astrophysics and Space Science Library.
51. P. Judge, Observations of the solar chromosphere. *Astron. Soc. Pac. Conf. Ser.* **354**, 259 (2006).
52. J. M. Fontenla, E. H. Avrett, R. Loeser, Energy balance in the solar transition region. III. Helium emission in hydrostatic, constant-abundance models with diffusion. *Astrophys. J.* **406**, 319 (1993).
53. A. Sainz Dalda, J. de la Cruz Rodríguez, B. De Pontieu, M. Gošić, Recovering thermodynamics from spectral profiles observed by IRIS: A machine and deep learning approach. *Astrophys. J. Lett.* **875**, L18 (2019).
54. J. de la Cruz Rodríguez, J. Leenaarts, S. Danilovic, H. Uitenbroek, STiC: A multiatom non-LTE PRD inversion code for full-Stokes solar observations. *Astron. Astrophys.* **623**, A74 (2019).
55. H. Socas-Navarro, J. Trujillo Bueno, B. Ruiz Cobo, Non-LTE inversion of stokes profiles induced by the Zeeman effect. *Astrophys. J.* **530**, 977–993 (2000).
56. J. M. da Silva Santos, J. de la Cruz Rodríguez, J. Leenaarts, Temperature constraints from inversions of synthetic solar optical, UV, and radio spectra. *Astron. Astrophys.* **620**, A124 (2018).
57. J. M. da Silva Santos, J. de la Cruz Rodríguez, J. Leenaarts, G. Chintzoglou, B. De Pontieu, S. Wedemeyer, M. Szydlarski, The multi-thermal chromosphere. Inversions of ALMA and IRIS data. *Astron. Astrophys.* **634**, A56 (2020).
58. J. de la Cruz Rodríguez, H. Socas-Navarro, M. Carlsson, J. Leenaarts, Non-local thermodynamic equilibrium inversions from a 3D magnetohydrodynamic chromospheric model. *Astron. Astrophys.* **543**, A34 (2012).

Acknowledgments: CLASP2 is an international partnership between NASA/MSFC, NAOJ, JAXA, IAC, and IAS; additional partners include ASCR, IRSOL, LMSAL, and the University of Oslo. The CLASP2 team acknowledges S. Ishikawa, who led the development of the critical component of the polarization modulation unit (PMU) at ISAS/JAXA. Hinode is a Japanese mission developed and launched by ISAS/JAXA, with NAOJ as domestic partner and NASA and STFC (UK) as international partners. It is operated by these agencies in cooperation with ESA and NSC (Norway). IRIS is a NASA Small Explorer Mission developed and operated by LMSAL with mission operations executed at NASA Ames Research Center and major contributions to downlink communications funded by ESA and the Norwegian Space Centre. **Funding:** The Japanese participation was funded by JAXA as a Small Mission-of-Opportunity Program, JSPS KAKENHI grant numbers JP25220703 and JP16H03963, 2015 ISAS Grant for Promoting International Mission Collaboration, and 2016 NAOJ Grant for Development Collaboration. The U.S. participation was funded by NASA Award 16-HTIDS16_2-0027. The Spanish participation was funded by the European Research Council (ERC) under the European Union's Horizon 2020 research and innovation program (Advanced Grant agreement no. 742265). The French hardware participation was funded by CNES funds CLASP2-13616A and 13617A. R.I. acknowledges the NAOJ Overseas Visit Program for Young Researchers (FY2019) and a Grant-in-Aid for Early-Career Scientists JP19K14771. J.T.B. acknowledges the funding received from the European Research Council through Advanced Grant agreement no. 742265. E.A.B. and L.B. acknowledge the funding received from the Swiss National Science Foundation through grants 200021-175997 and CRSII5-180238. B.D.P. and A.S.D. acknowledge support from NASA contract NNG09FA40C (IRIS). J.Š. acknowledges financial support by the Grant Agency of the Czech Republic through grant 19-20632S and project RVO:67985815. M.C. acknowledges support from the Research Council of Norway through its Centres of Excellence scheme, project number 262622, and through grants of computing time from the Programme for Supercomputing. **Author contributions:** R.I. and J.T.B. conceived the investigation, critically discussed each development step, and wrote the manuscript. R.I. led the data analysis, while J.T.B. and T.d.P.A. led the theoretical investigations applied to this study, which included discussions with E.A.B., L.B., J.Š., and A.A.R. The comparison between the CLASP2 and IRIS data was done by T.J.O., who also processed the Hinode/SOT data. D.E.M., R.I., J.T.B., and F.A. are the CLASP2 Principal Investigators from the United States, Japan, Spain, and France, respectively. T.J.O. and L.A.R., the CLASP2 project scientists, helped to coordinate the observations with IRIS and Hinode. B.D.P. conducted the IRIS observation and together with A.S.D. performed the inversions based on the IRIS[2] database. C.B., T.J.O., and D.S. contributed to the data calibration. R.K., D.S., M.Y., K.K., H.H., M.K., N.N., T.Sa., T.Sh., Y.S., G.D.V., and A.W. contributed to the development of the instrument. M.C. and J.L. provided information on models of the solar chromosphere. **Competing interests:** The authors declare that they have no competing interests. **Data and materials availability:** All data needed to evaluate the conclusions in the paper are present in the paper and/or the Supplementary Materials. The calibrated CLASP2 data will be made publicly available soon through the Virtual Solar Observatory. The Level 2 Hinode/SOT-SP data are available at https://csac.hao.ucar.edu/sp_data.php, the IRIS data are available at https://iris.lmsal.com/data.html, and the SDO data are available at http://jsoc.stanford.edu.

Submitted 17 September 2020
Accepted 8 January 2021
Published 19 February 2021
10.1126/sciadv.abe8406

Citation: R. Ishikawa, J. Trujillo Bueno, T. del Pino Alemán, T. J. Okamoto, D. E. McKenzie, F. Auchère, R. Kano, D. Song, M. Yoshida, L. A. Rachmeler, K. Kobayashi, H. Hara, M. Kubo, N. Narukage, T. Sakao, T. Shimizu, Y. Suematsu, C. Bethge, B. De Pontieu, A. Sainz Dalda, G. D. Vigil, A. Winebarger, E. Alsina Ballester, L. Belluzzi, J. Štěpán, A. Asensio Ramos, M. Carlsson, J. Leenaarts, Mapping solar magnetic fields from the photosphere to the base of the corona. *Sci. Adv.* **7**, eabe8406 (2021).

ScienceAdvances

Mapping solar magnetic fields from the photosphere to the base of the corona

Ryohko IshikawaJavier Trujillo BuenoTanausú del Pino AlemánTakenori J. OkamotoDavid E. McKenzieFrédéric AuchèreRyouhei KanoDonguk SongMasaki YoshidaLaurel A. RachmelerKen KobayashiHirohisa HaraMasahito KuboNoriyuki NarukageTaro SakaoToshifumi ShimizuYoshinori SuematsuChristian BethgeBart De PontieuAlberto Sainz DaldaGenevieve D. VigilAmy WinebargerErnest Alsina BallesterLuca BelluzziJi#í Št#pánAndrés Asensio RamosMats CarlssonJorrit Leenaarts

Sci. Adv., 7 (8), eabe8406. • DOI: 10.1126/sciadv.abe8406

Science Advances (ISSN 2375-2548) is published by the American Association for the Advancement of Science. 1200 New York Avenue NW, Washington, DC 20005. The title *Science Advances* is a registered trademark of AAAS.